Airy-based static limit analysis of structures using stabilized radial point interpolation method

Le Van Canh[1*], Ho Le Huy Phuc[1], Nguyen Hoang Phuong[1]

[1]International University, Vietnam National University - HCMC, Vietnam
*Corresponding author: lvcanh@hcmiu.edu.vn

ARTICLE INFO

DOI:10.46223/HCMCOUJS.tech.en.12.1.2020.2022

Received: July 30th, 2021

Revised: September 08th, 2021

Accepted: September 11th, 2021

Keywords:

airy stress function; radial point interpolation method; SCNI; SOCP; static limit analysis

ABSTRACT

This paper presents a novel formulation for static limit analysis of structures, for which the Airy stress function is approximated using stabilized Radial Point Interpolation Mesh-free method (RPIM). The stress field is determined as second-order derivatives of the Airy function, and the equilibrium equations are automatically satisfied a priori. The so-called Stabilized Conforming Nodal Integration (SCNI) is employed to ensure a present method is truly a mesh-free approach, meaning that all constraints in problems are only enforced at nodes. With the use of the Airy function, SCNI, and Second-Order Cone Programming (SOCP), the size of the resulting problem is kept to be minimum. Several benchmark problems having arbitrary geometries and boundary conditions are investigated. The obtained numerical solutions are compared with those available in other studies to perform the computational aspect of the proposed method.

1. Introduction

The estimation of limit load plays a crucial role in structural design. Originally, analytical approaches and numerous methods such as yield line, slip line, or strip approaches were widely used. However, in engineering practice, these procedures are incapable of handling the structures with complicated geometries and loading conditions, which require large numerical computations. Consequently, numerical methods based on bound theories and mathematical programming have been developed in the last few decades. Various numerical discretization schemes and mathematical algorithms have been proposed in the framework of limit analysis. Finite Element Methods (FEM) are well-known as the most commonly used tools in this field. There are three basic types of finite element models, i.e., displacement, equilibrium, and mixed formulations, for which the contributions can be found in Hodge and Belytschko (1968), Belytschko and Hodge (1970), Nguyen (1976), Pixin, Mingwan, and Kehchih (1991), Capsoni and Corradi (1997), Christiansen and Andersen (1999), Andersen, Christiansen, and Overton (1998), Capsoni (1999), Krabbenhoft and Damkilde (2003), Yu and Tin-Loi (2006), Le, Gilbert, and Askes (2010), Bleyer and De Buhan (2013). However, the creation of the mesh playing an important role in FEM implementation takes most of the total computational cost. There are several issues generated by the mesh; for example, in fracture problems, FEM may fail in handling the discontinuities at crack paths and crack tips; or in large deformation problems, for which the continuous meshing of the domain is required, the very fine mesh is needed, increasing the cost. The low order of shape function is also an obstacle of FEM. For instance, dealing with the equilibrium equations in static formulation, the Airy stress function, known as one of the most efficient treatments, is usually applied. The stress field is approximated by second-order derivatives of the Airy function, which cannot be obtained using FEM. Consequently, novel approaches, so-called mesh-free methods, have been continuously developed and significantly devoted to the development of limit analysis in recent years. Various meshless models have successfully applied to this area, for instance, Element-Free Galerkin (EFG) method (S. Chen, Liu, & Cen, 2008; Le, Gilbert, & Askes, 2009; Le et al., 2010; Le, Askes, & Gilbert, 2012; Le, Ho, & Nguyen, 2016), Natural Element Method (NEM) (S. T. Zhou & Liu, 2012; S. Zhou, Liu, & Chen, 2012), Radial Point Interpolation Method (RPIM) (F. Liu & Zhao, 2013; Mohapatra & Kumar, 2019), integrated Radial Basis Function (iRBF) method (Ho, Le, & Tran, 2016; Ho, Le, & Tran, 2018; Ho & Le, 2020; Ho, Le, & Nguyen, 2021). Dealing with the optimization problems, a number of optimization tools have been developed, such as linear programming (Nguyen, 1984; Sloan, 1988), linearizing yield surfaces (Maier, 1970; Tin-Loi, 1990), Newton algorithm (Andersen, 1996; Gaudrat, 1991), or primal-dual interior-point method (G. R. Liu & Karamanlidis, 2003; Nesterov & Nemirovskii, 1994).

In this study, a novel equilibrium formulation for limit state analysis of structures is developed. The Airy stress function is approximated using stabilized RPIM method (Ho, Le, & Phan, 2020), obtained by combining the original RPIM (G. R. Liu & Karamanlidis, 2003) and SCNI scheme (J. S. Chen, Wu, Yoon, & You, 2001). The SCNI method allows the numerical integration to be performed at nodes only and hence reduces the computational cost. The stress field is determined as the second derivative of the Airy function, leading to only one stress variable being needed per node. With the use of the Airy function, the equilibrium equations are satisfied priorly, meaning that they can be eliminated in the formulated problems. The stabilized RPIM method is a truly mesh-free; hence, the constraints in problems are only enforced at nodes. The optimization problem, which is kept in minimum size, is cast as SOCP and rapidly solved using the Mosek software package (MOSEK ApS, 2019).

2. Airy-based static formulation of limit analysis

Consider a rigid-perfectly plastic body of area Ω with kinematic boundary Γ_u, static boundary Γ_t, and subjected to the body force b, to the external pressure t. A statically admissible stress field is assumed, and the lower bound of the limit load multiplier will be obtained if the equilibrium conditions are satisfied and the yield criterion is not violated everywhere. The mathematical formulation of lower bound limit analysis can be expressed as follows

$$\lambda = \max \lambda^{-}$$
$$\text{s.t} \begin{cases} \nabla\sigma = 0, & \text{in } \Omega \\ \boldsymbol{n}\sigma = t, & \text{on } \Gamma_t \\ \psi(\sigma) \le 0, & \text{in } \Omega \end{cases} \tag{1}$$

where ∇ is differential operator, $\boldsymbol{n}$ is an outward surface normal matrix, $\psi(\sigma)$ is the yield function. In this study, the von Mises yield criterion is used, and the failure function can be given as

$$\psi(\sigma) = \begin{cases} \sqrt{\sigma_{xx}^2 + \sigma_{yy}^2 + \sigma_{xx}\sigma_{yy} + 3\sigma_{xy}^2} - \sigma_p, & \text{for plane stress} \\ \sqrt{\frac{1}{4}\left(\sigma_{xx} + \sigma_{yy}\right)^2 + \sigma_{xy}^2} - \sigma_p, & \text{for plane strain} \end{cases} \tag{2}$$

with (σ_{xx}, σ_{yy}, σ_{xy}) denotes stress components, σ_p is plastic stress of material.

The stress field must satisfy the following equilibrium condition

$$\nabla\sigma(x) + f = 0, \quad \forall \mathrm{x} \in \Omega \tag{3}$$

The body force can be derived from a potential function V as

$$f = -\nabla V \tag{4}$$

If the stress fields in two dimensions are determined based on Airy stress function φ as

$$\sigma_{xx} = \frac{\partial^2 \varphi}{\partial y^2} + V,\quad \sigma_{yy} = \frac{\partial^2 \varphi}{\partial x^2} + V,\quad \sigma_{xy} = -\frac{\partial^2 \varphi}{\partial x \partial y} \tag{5}$$

The equilibrium equation (3) is automatically satisfied a prior, as demonstrated in the following

$$\frac{\partial \sigma_{xx}}{\partial x} + \frac{\partial \sigma_{xy}}{\partial y} + f_x = \frac{\partial\left(\frac{\partial^2 \varphi}{\partial y^2} + V\right)}{\partial x} - \frac{\partial\left(\frac{\partial^2 \varphi}{\partial x \partial y}\right)}{\partial y} - \frac{\partial V}{\partial x} = 0$$

$$\frac{\partial \sigma_{xy}}{\partial x} + \frac{\partial \sigma_{yy}}{\partial y} + f_y = -\frac{\partial\left(\frac{\partial^2 \varphi}{\partial x \partial y}\right)}{\partial x} + \frac{\partial\left(\frac{\partial^2 \varphi}{\partial x^2} + V\right)}{\partial y} - \frac{\partial V}{\partial y} = 0 \tag{6}$$

With the absence of body force, the stress components can be rewritten as

$$\sigma_{xx} = \frac{\partial^2 \varphi}{\partial y^2},\quad \sigma_{yy} = \frac{\partial^2 \varphi}{\partial x^2},\quad \sigma_{xy} = -\frac{\partial^2 \varphi}{\partial x \partial y} \tag{7}$$

The principle of the lower bound limit formulation can be now rewritten as follows

$$\begin{aligned} &\lambda = \max \lambda^- \\ &\text{s.t} \begin{cases} \boldsymbol{n}\sigma = t, & \text{on } \Gamma_t \\ \psi(\sigma) \le \sigma_p, & \text{in } \Omega \end{cases} \end{aligned} \tag{8}$$

It is noted that using Airy function, three stress components (σ_{xx}, σ_{yy}, σ_{xy}) can be calculated via stress function $\varphi(\sigma)$ as seen in Equation (7), meaning that only function $\varphi(\sigma)$ need to be approximate. In addition, the approximated stress function has to satisfy static boundary conditions and yield function only.

3. Radial point interpolation mesh-free method

The approximate function for a set of scattered nodes $\boldsymbol{x}_Q^T = [x_1, x_2, \ldots, x_N] \in \Omega$ is obtained by interpolating pass through nodal value as

$$u^h(\boldsymbol{x}) = \boldsymbol{R}(\boldsymbol{x})\boldsymbol{a} + \boldsymbol{p}(\boldsymbol{x})\boldsymbol{b} \tag{9}$$

where $\boldsymbol{a}^T = \{a_1, a_2, \ldots, a_N\}$ and $\boldsymbol{b}^T = \{b_1, b_2, \ldots, b_M\}$ are the coefficient vectors related to radial basis function (RBF) $\boldsymbol{R}(\boldsymbol{x})$ and polynomial basis function (PBF) $\boldsymbol{p}(\boldsymbol{x})$, respectively, N is a number of nodes in the computational domain, M is a number of terms in $\boldsymbol{p}(\boldsymbol{x})$.

The matrix form of Equation (9) when enforcing $u^h(\boldsymbol{x})$ at scattered nodes in a problem domain can be expressed as follows

$$\boldsymbol{U} = \boldsymbol{R}_Q\boldsymbol{a} + \boldsymbol{P}_M\boldsymbol{b} \tag{10}$$

where $\boldsymbol{R}_Q$ is given by

$$\boldsymbol{R}_Q = \begin{bmatrix} \cdots & \cdots & \cdots & \cdots \\ R_1(r_k) & R_2(r_k) & \cdots & R_N(r_k) \\ \cdots & \cdots & \cdots & \cdots \end{bmatrix}_{N\times N} \tag{11}$$

with $r_k = \| \boldsymbol{x}_k - \boldsymbol{x}_I \|$ is the distance from the point I^{th} to node $\boldsymbol{x}_k$ within the set$\boldsymbol{x}_Q$. In this study, the best-ranked function in terms of accuracy, so-called Multi-Quadric (MQ), is employed

$$R_I(r_k) = \sqrt{r_k^2 + c_I^2} \tag{12}$$

where $c_I = \alpha_s d_I$ is the shape parameter with $\alpha_s > 0$ and d_I is the minimal distance from point $\boldsymbol{x}_I$ to its neighbors.

To guarantee the unique approximation of function, the polynomial term must satisfy the following condition

$$\boldsymbol{P}_M^T \boldsymbol{a} = 0 \tag{13}$$

The Equations (10) and (13) can be combined and rewritten as follows

$$\begin{bmatrix} \boldsymbol{R}_Q & \boldsymbol{P}_M \\ \boldsymbol{P}_M^T & \boldsymbol{0} \end{bmatrix} \begin{Bmatrix} \boldsymbol{a} \\ \boldsymbol{b} \end{Bmatrix} = \begin{Bmatrix} \boldsymbol{U} \\ \boldsymbol{0} \end{Bmatrix} \tag{14}$$

Or
$$\boldsymbol{G} \begin{Bmatrix} \boldsymbol{a} \\ \boldsymbol{b} \end{Bmatrix} = \begin{Bmatrix} \boldsymbol{U} \\ \boldsymbol{0} \end{Bmatrix} \tag{15}$$

The coefficient vectors $\boldsymbol{a}$ and $\boldsymbol{b}$ can be computed in an efficient manner (G. R. Liu & Karamanlidis, 2003) as

$$\boldsymbol{a} = \boldsymbol{R}_Q^{-1}\boldsymbol{U} - \boldsymbol{R}_Q^{-1}\boldsymbol{P}_M\boldsymbol{b}; \quad \boldsymbol{b} = \chi_b \boldsymbol{U} \tag{16}$$

where

$$\chi_b = [\boldsymbol{P}_M^T \boldsymbol{R}_Q^{-1} \boldsymbol{P}_M]^{-1} \boldsymbol{P}_M^T \boldsymbol{R}_Q^{-1} \tag{17}$$

Substituting $\boldsymbol{b}$ to Equation (13), vector $\boldsymbol{a}$ can be obtained by

$$\boldsymbol{a} = \chi_a \boldsymbol{U} \tag{18}$$

where

$$\chi_a = \boldsymbol{R}_Q^{-1}[1 - \boldsymbol{P}_M \chi_b] = \boldsymbol{R}_Q^{-1} - \boldsymbol{R}_Q^{-1}\boldsymbol{P}_M \chi_b \tag{19}$$

The approximation function in Equation (6) can be now rewritten as

$$u^h(\boldsymbol{x}) = [\boldsymbol{R}(\boldsymbol{x})\chi_a + \boldsymbol{p}(\boldsymbol{x})\chi_b]\boldsymbol{U} = \sum_{I=1}^{N} \Phi_I(\boldsymbol{x}) u_I \tag{20}$$

The shape function and its partial derivatives for node k^{th} can be expressed as

$$\Phi_k = \sum_{I=1}^{N} R_I \chi_{Ik}^a + \sum_{J=1}^{M} p_J \chi_{Jk}^b \tag{21}$$

$$\frac{\partial \Phi_k}{\partial x} = \sum_{I=1}^{N} \frac{\partial R_I}{\partial x} \chi_{Ik}^a + \sum_{J=1}^{M} \frac{\partial p_J}{\partial x} \chi_{Jk}^b; \quad \frac{\partial \Phi_k}{\partial y} = \sum_{I=1}^{N} \frac{\partial R_I}{\partial y} \chi_{Ik}^a + \sum_{J=1}^{M} \frac{\partial p_J}{\partial y} \chi_{Jk}^b \tag{22}$$

To improve the computational aspect and ensure the proposed method are truly mesh-free procedure, the Stabilized Conforming Nodal Integration (SCNI) scheme introduced in J. S. Chen et al. (2021) is employed in this study. The idea of SCNI is that strains will be smoothed over the representative domain as follows

$$\tilde{\varepsilon}_{ij}^h(\boldsymbol{x}_J) = \frac{1}{a_J}\int_{\Omega_J} \frac{1}{2}(u_{i,j}^h + u_{j,i}^h) d\Omega = \frac{1}{2a_J}\oint_{\Gamma_J} \left(u_i^h n_j + u_j^h n_i\right) d\Omega \tag{23}$$

where $\tilde{\varepsilon}_{ij}^h$ is the smoothed strains at node J; u_i and u_j are displacement components; a_J and Γ_J are area and boundary of a representative domain Ω_J; n_i and n_j are outward normal of edges bounding domain Ω_JAs shown in Figure 1.

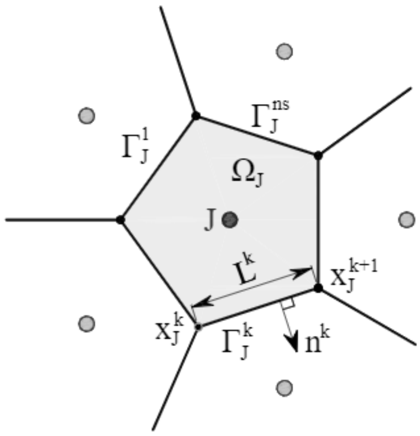

Figure 1. Geometry definition of a nodal representative domain

The smooth version of strains can be now expressed as

$$\varepsilon^h(\boldsymbol{x}_J) = \left[\tilde{\varepsilon}_{xx}^h(\boldsymbol{x}_J) \quad \tilde{\varepsilon}_{yy}^h(\boldsymbol{x}_J) \quad 2\tilde{\varepsilon}_{xy}^h(\boldsymbol{x}_J)\right]^T = \widetilde{\boldsymbol{B}}\boldsymbol{d} \tag{24}$$

where $\boldsymbol{d}$ denotes the displacement vector and $\widetilde{\boldsymbol{B}}$ is the displacement-strain matrix consisting of the smoothed derivatives of shape function

$$\widetilde{\Phi}_{I,\alpha}(\boldsymbol{x}_J) = \frac{1}{a_J}\oint_{\Gamma_J} \Phi_I(\boldsymbol{x}_J) n_\alpha(\boldsymbol{x}) d\Gamma = \frac{1}{2a_J}\sum_{k=1}^{ns} (n_\alpha^k\, L^k + n_\alpha^{k+1}\, L^{k+1})\Phi_I(\boldsymbol{x}_J^{k+1}) \tag{25}$$

where $\widetilde{\Phi}$ is the smoothed version of Φ; ns is the number of edges; $\boldsymbol{x}_J^k$ and $\boldsymbol{x}_J^{k+1}$ are the coordinates of the two endpoints of the boundary segment Γ_J^k having length L^k and outward surface normal n^k.

Similarly, the smoothed version of second-order derivatives of shape function can be calculated from the first-order ones as

$$\begin{aligned}\tilde{\Phi}_{I,\alpha\beta}(\boldsymbol{x}_J) &= \frac{1}{2A_J}\oint_{\Gamma_J}\left[\Phi_{I,\alpha}(\boldsymbol{x}_J)n_\beta(\boldsymbol{x}) + \Phi_{I,\beta}(\boldsymbol{x}_J)n_\alpha(\boldsymbol{x})\right]\mathrm{d}\Omega \\ &= \frac{1}{4A_J}\sum_{k=1}^{ns}\left(n_\beta^k L^k + n_\beta^{k+1}L^{k+1}\right)\Phi_{I,\alpha}\left(\boldsymbol{x}_J^{k+1}\right) \\ &+ \frac{1}{4A_J}\sum_{k=1}^{ns}\left(n_\alpha^k L^k + n_\alpha^{k+1}L^{k+1}\right)\Phi_{I,\beta}\left(\boldsymbol{x}_J^{k+1}\right)\end{aligned} \tag{26}$$

with $\Phi_{I,\alpha}$ and $\Phi_{I,\beta}$ are the first-order derivatives of shape function relating to variables α and β.

It is worth noting that the RPIM shape function possesses the Kronecker delta property, leading to the essential boundary conditions can be easily imposed in a similar way to the finite element method. Furthermore, using the stabilized shape function, the constraints in formulated problems are enforced at nodes, yielding the reduction of computational cost.

4. RPIM discretisation of lower bound limit analysis

The Airy stress function is approximated using the RPIM method as follows

$$\varphi(\sigma) = \sum_{I=1}^{N} \Phi_I(x)\sigma_I \tag{27}$$

where $\Phi_I(x)$ and σ_I are RPIM shape function and nodal reflection of approximated function $\varphi(\sigma)$ at node I^{th}, respectively.

The stress components at node I^{th} can be expressed by second-order derivatives of $\varphi(\sigma)$ as

$$\begin{aligned}
\sigma_{xx} &= \frac{\partial^2 \varphi}{\partial y^2} = \sum_{I=1}^{N} \tilde{\Phi}_{I,yy}(\boldsymbol{x})\sigma_I \\
\sigma_{yy} &= \frac{\partial^2 \varphi}{\partial x^2} = \sum_{I=1}^{N} \tilde{\Phi}_{I,xx}(\boldsymbol{x})\sigma_I \\
\sigma_{xy} &= -\frac{\partial^2 \varphi}{\partial x \partial y} = -\sum_{I=1}^{N} \tilde{\Phi}_{I,xy}(\boldsymbol{x})\sigma_I
\end{aligned} \tag{28}$$

where $\widetilde{\Phi}_{I,xx}(x)$, $\widetilde{\Phi}_{I,yy}(x)$ and $\widetilde{\Phi}_{I,xy}(x)$ are smoothed versions of second-order derivatives of the RPIM shape function.

Note that stresses determined by equation (28) automatically satisfy equilibrium equation (3), as demonstrated in equations (4-6).

It can be observed that the number of variables in the problem is kept to be minimum owing to three stress components $(\sigma_{xx}, \sigma_{yy}, \sigma_{xy})$ are performed via only one nodal reflection σ_IReducing the computational cost significantly.

The stress field can be now presented as

$$\sigma^h(x) = \begin{bmatrix}\sigma^h_{xx} & \sigma^h_{yy} & \sigma^h_{xy}\end{bmatrix}^T = Cs \tag{29}$$

where

$$C = \begin{bmatrix} C_{xx} \\ C_{yy} \\ C_{xy} \end{bmatrix} = \begin{bmatrix} \widetilde{\Phi}_{1,yy} & \widetilde{\Phi}_{2,yy} & \cdots & \widetilde{\Phi}_{N,yy} \\ \widetilde{\Phi}_{1,xx} & \widetilde{\Phi}_{2,xx} & \cdots & \widetilde{\Phi}_{N,xx} \\ \widetilde{\Phi}_{1,xy} & \widetilde{\Phi}_{2,xy} & \cdots & \widetilde{\Phi}_{N,xy} \end{bmatrix}; \quad \mathrm{s}^T = [\sigma_1 \quad \sigma_2 \quad \cdots \quad \sigma_N] \tag{30}$$

The approximated stress field must belong to the convex domain $\mathcal{B}$, for which the von Mises yield criterion is rewritten in terms of a sum of norms as follows

$$\mathcal{B} \equiv \begin{cases} \mathcal{L}_{PS} = \left\{\rho \in \mathbb{R}^3 \;\mid\; \rho_1 \geq \|\rho_{2\to4}\|^2_L = \sqrt{\rho_2^2 + \rho_3^2 + \rho_4^2}\right\}, & \text{for plane stress} \\ \mathcal{L}_{PD} = \left\{\rho \in \mathbb{R}^3 \;\mid\; \rho_1 \geq \|\rho_{2\to3}\|^2_L = \sqrt{\rho_2^2 + \rho_3^2}\right\} & \text{For plane strain} \end{cases} \tag{31}$$

where the additional variables $(\rho_1, \rho_2, \rho_3, \rho_4)$ are given by

$$\begin{aligned}
\rho_1 &= \sigma_p \\
\rho_{2\to4} &= \begin{bmatrix}\rho_2 \\ \rho_3 \\ \rho_4\end{bmatrix} = \frac{1}{2}\begin{bmatrix} 2 & 0 & 0 \\ -1 & \sqrt{3} & 0 \\ 0 & 0 & 2\sqrt{3}\end{bmatrix} Cs, \quad \text{for plane stress} \\
\rho_{2\to3} &= \begin{bmatrix}\rho_2 \\ \rho_3\end{bmatrix} = \frac{1}{2}\begin{bmatrix} C_{xx} - C_{yy} \\ 2\,C_{xy}\end{bmatrix} s, \quad \text{for plane strain}
\end{aligned} \tag{32}$$

The optimization problem (8) can be now formulated as SOCP form as

$$\begin{aligned}
&\lambda = \max \lambda^- \\
&\text{s.t} \begin{cases} \boldsymbol{Cs} = t, & \text{on } \Gamma_t \\ \rho^k \in \mathcal{B} & k = 1, 2, \ldots, N_p \end{cases}
\end{aligned} \tag{33}$$

where N_p is number of integration points.

It is interesting to note that, using SCNI, the equilibrium equations in (3) and all constraints in (33) are fully satisfied everywhere in the problem domain, but in average-sense. Therefore, the solution obtained from (33) may not be guaranteed to represent a strict lower-bound on the exact value. However, the reliable approximation of actual collapse load multipliers can be achieved using a sufficiently fine nodal mesh.

5. Numerical results

In this section, several benchmark plane stress and plane strain problems governed by von Mises yield criterion are investigated to examine the computational effect of the proposed method. The shape parameter $\alpha_s = 10^{-5}$and the radius of support domain $R_s = 3d_I$ are chosen for all problems. The resulting optimization problems are solved using Mosek optimization solver version 9.0 integrated into the Matlab environment on a 2.8 GHz Intel Core i7 PC running Window 10.

5.1. Double notched specimen in tension

This example deals with a well-known problem in-plane strain, consisting of a rectangular plate having double cracks at boundaries and subjected to tension load, as shown in Figure 2(a). With the given data $W = L$, the problem is considered in three cases: $a = \frac{L}{3}, a = \frac{L}{2}, a = \frac{2L}{3}$. Owing to the symmetry, the upper-right quarter of the plate, for which the dimensions and boundary conditions are illustrated in Figure 2(b), is modeled. The nodal discretization for the mesh of 169 nodes and related representative domains created using Voronoi diagrams are also plotted in Figure (2c).

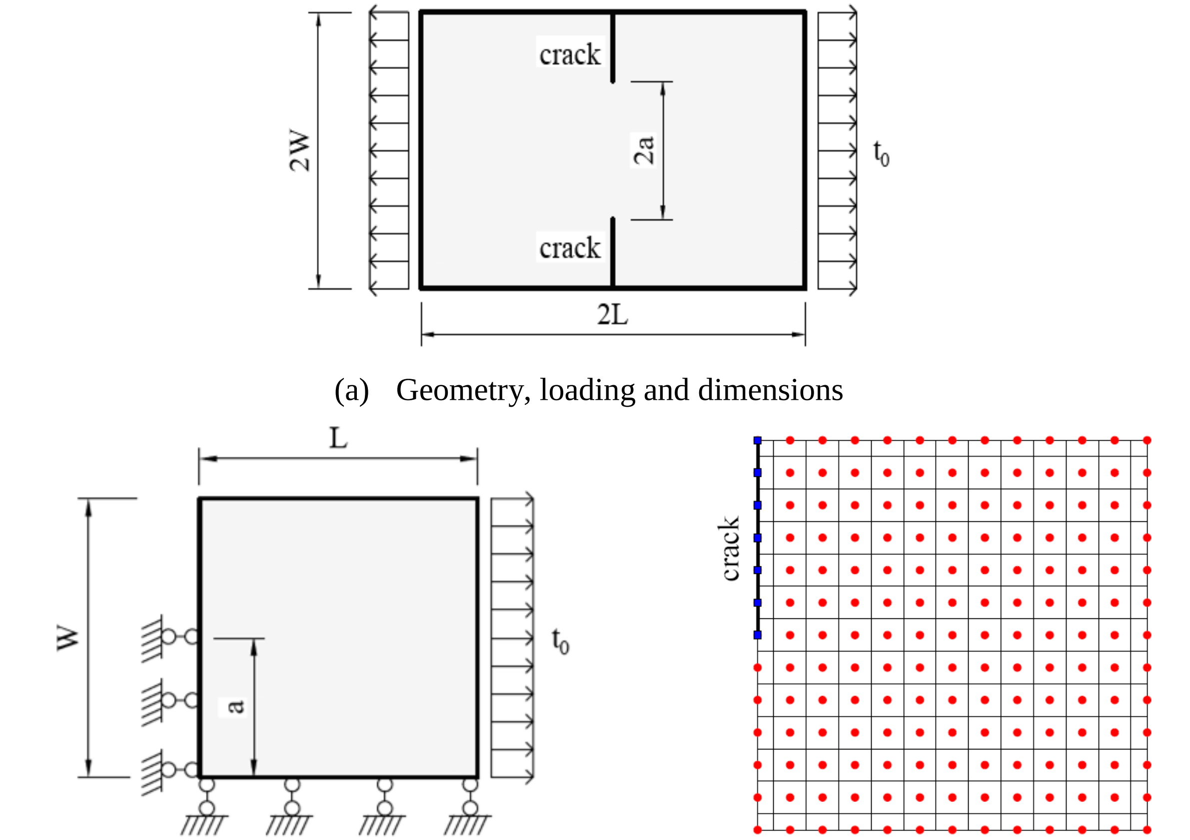

(b) Computational domain and boundary conditions

(c) Nodal discretization and representative domains

Figure 2. Double notched specimen problem

Table 1 presents the collapse load multipliers obtained using the proposed RPIM procedure, in which different types of polynomial basis functions are employed. The convergence analysis and comparison are also plotted in Figure 3. It can be observed that, with the use of equilibrium formulation, the limit load factors increase when increasing number of nodes or variables. Among four types of PBF used, the RPIM approximation obtained by combining radial basis function and cubic polynomial one results in the best accurate and stable solutions. The size of an optimization problem is reduced significantly owing to the combination of Airy stress function and SOCP. Consequently, the problem with thousand variables can be rapidly solved in a few seconds, as seen in Table 1.

Table 1

Double notched specimen: the convergence of limit load multipliers

Model	Number of nodes (N_{var})				
	169 (677)	361 (1445)	625 (2501)	961 (3845)	1369 (5477)
$a = \frac{L}{3}$	0.850	0.894	0.915	0.921	0.922
CPU-time (s)	< 1	< 1	< 1	< 1	1
$a = \frac{L}{2}$	1.066	1.109	1.118	1.128	1.131
CPU-time (s)	< 1	< 1	< 1	< 1	1
$a = \frac{2L}{3}$	1.303	1.346	1.366	1.374	1.381
CPU-time (s)	< 1	< 1	< 1	< 1	1

N_{var} is the number of variables in an optimization problem

Source: Data analysis result of the research

Table 2

Double notched specimen: the comparison with other studies

Author	Approach	Collapse load factors		
		$a = \frac{L}{3}$	$a = \frac{L}{2}$	$a = \frac{2L}{3}$
Present method	Static	0.922	1.131	1.381
Krabbenhoft and Damkilde (2003)	Static	-	1.132	-
Le et al. (2016), *EFG-Airy*	Static	0.921	1.131	1.381
Ho et al. (2016), *iRBF*	Static	-	1.127	-
Le et al. (2010), *CS-FEM*	Kinematic	0.926	1.137	1.384
Le et al. (2012), *EFG*	Kinematic	0.941	1.154	1.410
Ho et al. (2016), *iRBF*	Kinematic	-	1.141	-
Christiansen and Andersen (1999)	Mixed formulation	0.926	1.136	1.388
Andersen et al. (1998)	Mixed formulation	0.927	1.137	1.389

Source: Data analysis result of the research

The problem has also been investigated in Krabbenhoft and Damkilde (2003), using static FEM, in Le et al. (2010) using kinematic CS-FEM, in Le et al. (2016) using equilibrium EFG formulation combined with Airy stress function, in Christiansen and Andersen (1999); Andersen et al. (1998) using mixed finite element formulation. The comparison of present solutions and previous ones are summarized in Table 2. Generally, present results are in good agreement with those available in other studies. From Table 2 and Figure 3, it can be observed that obtained collapse load factors are very close to ones reported in Le et al. (2016) using equilibrium EFG approach and Airy function, the relative errors for the cases of $\frac{a}{L} = \left[\frac{1}{3}, \frac{1}{2}, \frac{2}{3}\right]$ are 0.11%, 0% and 0%, respectively. However, it is worth noting that, with the use of RPIM approximation, in which the shape function satisfies Kronecker delta property, the matrices in formulated problems are spare; hence, the CPU-Time in this paper is less than those reported in Le et al. (2016) when using similar nodal discretization and number variables in resulting optimization problem.

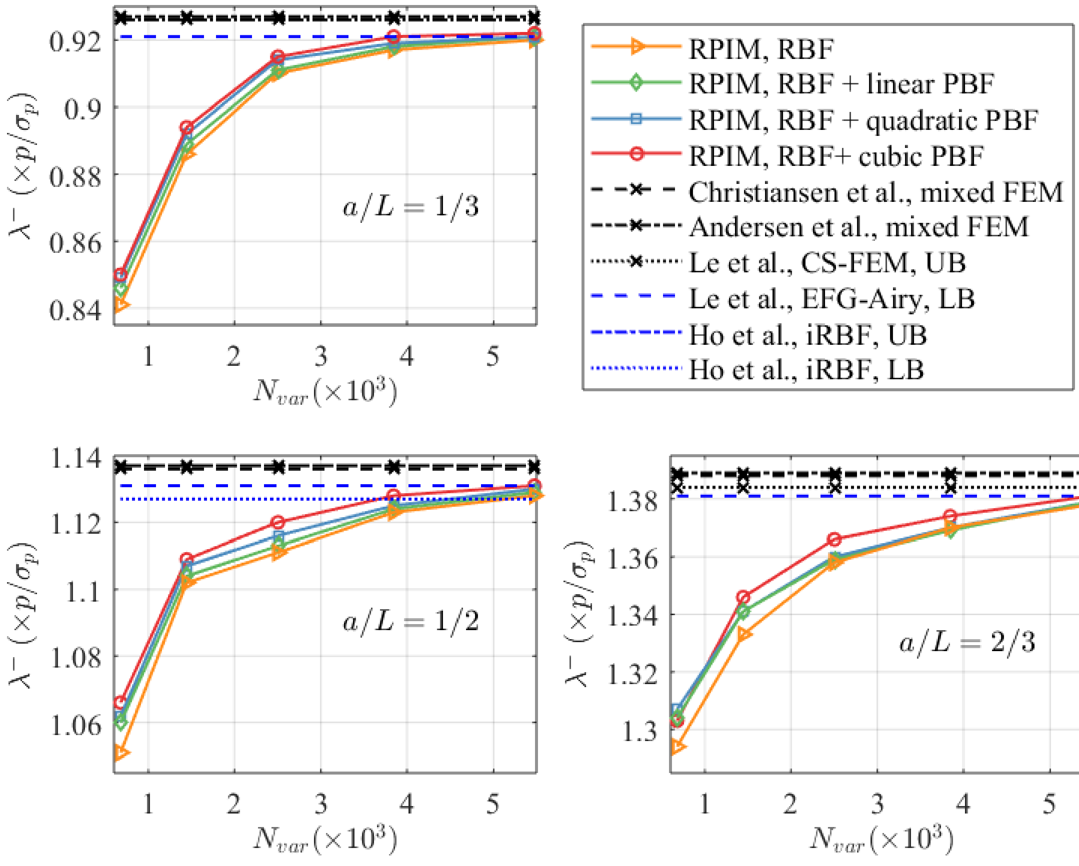

Figure 3. Double notched specimen: the convergence analysis with different values of $\frac{a}{L}$ (UB: Upper Bound, LB: Lower Bound)

5.2. Thin plate with square cutout subjected to tension

In this example, a plane stress thin plate with a rectangular cutout at the center subjected to a uniform tension load, as shown in Figure 4, is studied. Taking advantage of the symmetry, an only the upper-right quarter is modeled, see Figure (5a). The nodal discretization and representative domains are illustrated in Figure 5(b).

The collapse load multipliers associated with different nodal distributions are reported in Table 3 and plotted in Figure 6. Table 4 shows the comparison to other studies using kinematic and static formulations. The relative errors of the present solution and other those are small (almost less than 3%). The error of 6.64% compared with one reported in Belytschko and Hodge (1970) can be explained that the linear programming was used to solve the optimization problem in Belytschko and Hodge (1970); hence, the result is low accurate. It can be observed that the present lower bound collapse multiplier of 0.739 is higher (better) than ones of 0.693 in Belytschko and Hodge (1970), and in good agreement with available numerical ones in the literature.

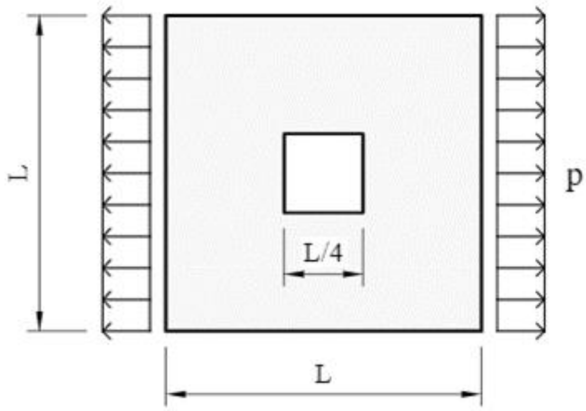

Figure 4. Square cutout plate

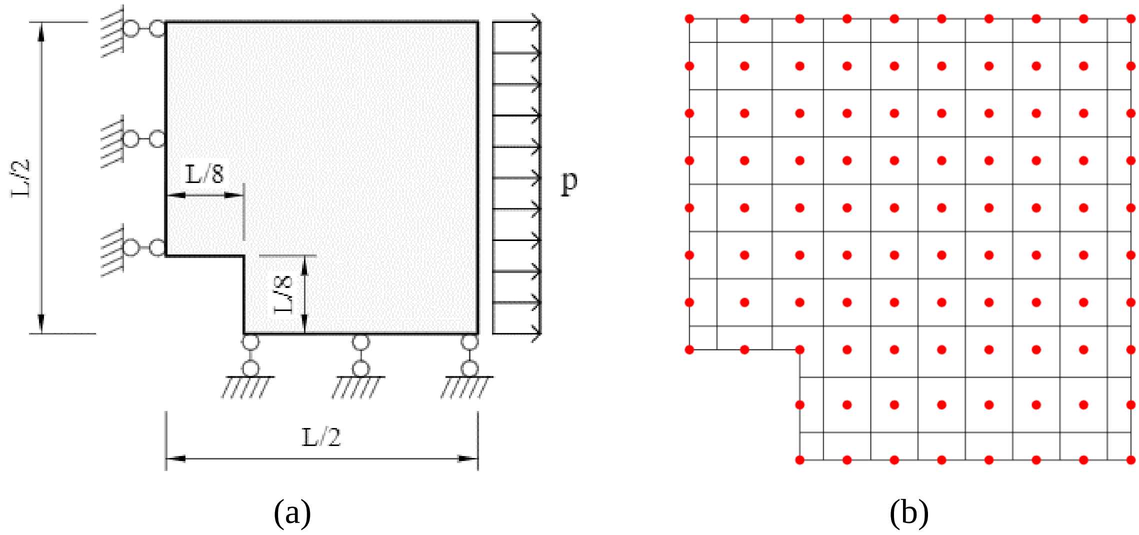

Figure 5. Square cutout plate: (a) Computational domain and boundary conditions, (b) Nodal discretization and representative domains

Table 3

Square cutout problem: Collapse load multipliers

Nodes	**60**	**160**	**308**	**540**	**792**	**1288**
N_{var}	301	801	1541	2701	3961	6441
$\lambda^{-}\left(\times\dfrac{p}{\sigma_p}\right)$	0.295	0.608	0.687	0.724	0.734	0.739
CPU-times (s)	< 1	< 1	< 1	< 1	1	2

N_{var} is the number of variables in an optimization problem

Source: Data analysis result of the research

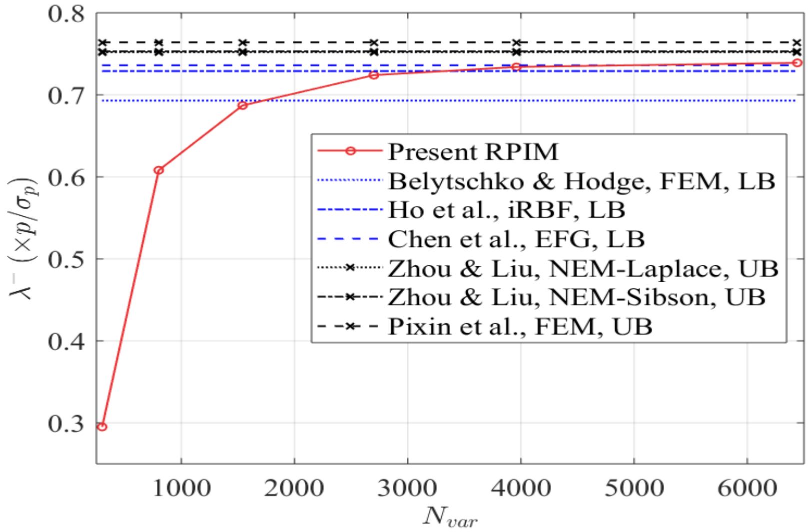

Figure 6. Square cutout problem: the convergence analysis

Table 4

Square cutout problem: The comparison with other studies

Author	Approach	$\lambda\left(\times\frac{p}{\sigma_p}\right)$	Errors (%)
Present method	Static	0.739	-
S. Chen et al. (2008), *EFG*	Static	0.736	0.41
Ho et al. (2016), *iRBF*	Static	0.729	1.37
Belytschko and Hodge (1970), *FEM*	Static	0.693	6.64
S. T. Zhou and Liu (2012), *NEM-Laplace*	Kinematic	0.752	1.73
S. T. Zhou and Liu (2012), *NEM-Sibson*	Kinematic	0.753	1.86
Pixin et al. (1991), *FEM*	Kinematic	0.764	3.27

Source: Data analysis result of the research

6. Conclusions

The present study has described an equilibrium mesh-free formulation based on stabilized radial point interpolation and Airy stress function. The truly mesh-free procedure is obtained owing to the use of the SCNI scheme, leading to the constraints in problems that only need to be enforced at scattered nodes. The stress field is performed via second derivatives of an approximated function, and the equilibrium conditions are satisfied automatically. By means of Airy function, SCNI and SOCP, the resulting optimization problems are kept at minimum size and solved rapidly. The good agreement of present solutions in comparison with those in other studies shows the computational efficiency of the proposed method.

ACKNOWLEDGEMENTS

This research is funded by Vietnam National University - HCMC (VNUHCMC) grant numbers B2018-28-04

References

Andersen, E. D., Roos, C., & Terlaky, T. (2003). On implementing a primal-dual interior-point method for conic quadratic optimization. *Mathematical Programming, 95*(2), 249-277.

Andersen, K. D. (1996). An efficient Newton barrier method for minimizing a sum of Euclidean norms. *SIAM Journal on Optimization*, *6*(1), 74-95.

Andersen, K. D., Christiansen, E., & Overton, M. L. (1998). Computing limit loads by minimizing a sum of norms. *SIAM Journal on Scientific Computing*, *19*(3), 1046-1062.

Belytschko, T., & Hodge, P. G. Jr. (1970). Plane stress limit analysis by finite elements. *Journal of the Engineering Mechanics Division*, *96*(6), 931-944.

Bleyer, J., & De Buhan, P. (2013). On the performance of non- conforming finite elements for the upper bound limit analysis of plates. *International Journal for Numerical Methods in Engineering*, *94*(3), 308-330.

Capsoni, A. (1999). A mixed finite element model for plane strain limit analysis computations. *Communications in Numerical Methods in Engineering, 15*(2), 101-112.

Capsoni, A., & Corradi, L. (1997). A finite element formulation of the rigid-plastic limit analysis problem. *International Journal for Numerical Methods in Engineering*, *40*(11), 2063-2086.

Chen, J. S., Wu, C. T., Yoon, S., & You, Y. (2001). A stabilized conforming nodal integration for Galerkin mesh- free methods. *International Journal for Numerical Methods in Engineering, 50*(2), 435-466.

Chen, S., Liu, Y., & Cen, Z. (2008). Lower-bound limit analysis by using the EFG method and non- linear programming. *International Journal for Numerical Methods in Engineering, 74*(3), 391-415.

Christiansen, E., & Andersen, K. D. (1999). Computation of collapse states with von Mises type yield condition. *International Journal for Numerical Methods in Engineering, 46*(8), 1185-1202.

Gaudrat, V. F. (1991). A Newton type algorithm for plastic limit analysis. *Computer Methods in Applied Mechanics and Engineering, 88*(2), 207-224.

Ho, P. L. H., & Le, C. V. (2020). A stabilized iRBF mesh-free method for quasi-lower bound shakedown analysis of structures. *Computers & Structures*, *228*(1), Article 16157.

Ho, P. L. H., Le, C. V., & Nguyen, P. H. (2021). Kinematic yield design computational homogenization of micro-structures using the stabilized iRBF mesh-free method. *Applied Mathematical Modelling, 91*(1), 322-334.

Ho, P. L. H., Le, C. V., & Phan, H. D. (2020). A computational homogenization analysis of materials using the stabilized mesh-free method based on the radial basis functions. *Journal of Science and Technology in Civil Engineering (STCE)-NUCE, 14*(1), 65-76.

Ho, P. L. H., Le, C. V., & Tran, T. C. (2016). Displacement and equilibrium mesh-free formulation based on integrated radial basis functions for dual yield design. *Engineering Analysis with Boundary Elements*, *71*(1), 92-100.

Ho, P. L. H., Le, C. V., & Tran, T. C. (2018). Limit state analysis of reinforced concrete slabs using an integrated radial basis function based mesh-free method. *Applied Mathematical Modelling, 53*(1), 1-11.

Hodge, P. G. Jr., & Belytschko, T. (1968). Numerical methods for the limit analysis of plates. *Journal of Applied Mechanics, 35*(4), 796-802.

Krabbenhoft, K., & Damkilde, L. (2003). A general non-linear optimization algorithm for lower bound limit analysis. *International Journal for Numerical Methods in Engineering, 56*(2), 165-184.

Le, C. V., Askes, H., & Gilbert, M. (2012). A locking-free stabilized kinematic EFG model for plane strain limit analysis. *Computers & Structures, 106*, 1-8.

Le, C. V., Gilbert, M., & Askes, H. (2009). Limit analysis of plates using the EFG method and second- order cone programming. *International Journal for Numerical Methods in Engineering, 78*(13), 1532-1552.

Le, C. V., Gilbert, M., & Askes, H. (2010). Limit analysis of plates and slabs using a meshless equilibrium formulation. *International Journal for Numerical Methods in Engineering, 83*(13), 1739-1758.

Le, C. V., Ho, P. L. H., & Nguyen, H. T. (2016). Airy-based equilibrium mesh-free method for static limit analysis of plane problems. *Vietnam Journal of Mechanics, 38*(3), 167-179.

Le, C. V., Nguyen, H. X., Askes, H., Bordas, S. P., Rabczuk, T., & Nguyen, H. V. (2010). A cell-based smoothed finite element method for kinematic limit analysis. *International Journal for Numerical Methods in Engineering, 83*(12), 1651-1674.

Liu, F., & Zhao, J. (2013). Upper bound limit analysis using radial point interpolation meshless method and nonlinear programming. *International Journal of Mechanical Sciences, 70*(1), 6-38.

Liu, G. R., & Karamanlidis, D. (2003). Mesh free methods: Moving beyond the finite element method. *Applied Mechanics Reviews, 56*(2), B17-B18.

Maier, G. (1970). A matrix structural theory of piecewise linear elastoplasticity with interacting yield planes. *Meccanica, 5*(1), 54-66.

Mohapatra, D., & Kumar, J. (2019). Collapse loads for rectangular foundations by three-dimensional upper bound limit analysis using radial point interpolation method. *International Journal for Numerical and Analytical Methods in Geomechanics, 43*(2), 641-660.

MOSEK ApS. (2019). *Mosek optimization toolbox for matlab*. Retrieved May 10, 2021, from http://docs.mosek.com/9.0/toolbox/index.html

Nesterov, Y., & Nemirovskii, A. (1994). *Interior-point polynomial algorithms in convex programming*. Philadelphia, PA: Society for industrial and applied mathematics.

Nguyen, H. D. (1976). Direct limit analysis via rigid-plastic finite elements. *Computer Methods in Applied Mechanics and Engineering, 8*(1), 81-116.

Nguyen, H. D. (1984). CEPAO - An automatic program for rigid-plastic and elastic-plastic analysis and optimization of frame structures. *Engineering Structures, 6*(1), 33-51.

Pixin, Z., Mingwan, L., & Kehchih, H. (1991). A mathematical programming algorithm for limit analysis. *Acta Mechanica Sinica, 7*(3), 267-274.

Sloan, S. W. (1988). Lower bound limit analysis using finite elements and linear programming. *International Journal for Numerical and Analytical Methods in Geomechanics, 12*(1), 61-77.

Tin-Loi, F. (1990). A yield surface linearization procedure in limit analysi. *Journal of Structural Mechanics, 18*(1), 135-149.

Yu, X., & Tin-Loi, F. (2006). A simple mixed finite element for static limit analysis. *Computers & Structures, 84*(29/30), 1906-1917.

Zhou, S. T., & Liu, Y. H. (2012). Upper-bound limit analysis based on the natural element method. *Acta Mechanica Sinica, 28*(5), 1398-1415.

Zhou, S., Liu, Y., & Chen, S. (2012). Upper bound limit analysis of plates utilizing the C1 natural element method. *Computational Mechanics, 50*(5), 543-561.